



Cite this: *Digital Discovery*, 2024, **3**, 2341

Sorting polyolefins with near-infrared spectroscopy: identification of optimal data analysis pipelines and machine learning classifiers^{†‡}

Bradley P. Sutliff, ^a Peter A. Beauchage, ^b Debra J. Audus, ^a Sara V. Orski ^a and Tyler B. Martin ^{*a}

Polyolefins (POs) are the largest class of polymers produced worldwide. Despite the intrinsic chemical similarities within this class of polymers, they are often physically incompatible. This combination presents a significant hurdle for high-throughput recycling systems that strive to sort various types of plastics from one another. Some research has been done to show that near-infrared spectroscopy (NIR) can sort POs from other plastics, but they generally fall short of sorting POs from one another. In this work, we enhance NIR spectroscopy-based sortation by screening over 12 000 machine-learning pipelines to enable sorting of PO species beyond what is possible using current NIR databases. These pipelines include a series of scattering corrections, filtering and differentiation, data scaling, dimensionality reduction, and machine learning classifiers. Common scattering corrections and preprocessing steps include scatter correction, linear detrending, and Savitzky–Golay filtering. Dimensionality reduction techniques such as principal component analysis (PCA), functional principal component analysis (fPCA) and uniform manifold approximation and projection (UMAP) were also investigated for classification enhancements. This analysis of preprocessing steps and classification algorithm combinations identified multiple data pipelines capable of successfully sorting PO materials with over 95% accuracy. Through rigorous testing, this study provides recommendations for consistently applying preprocessing and classification techniques without over-complicating the data analysis. This work also provides a set of preprocessing steps, a chosen classifier, and tuned hyperparameters that may be useful for benchmarking new models and data sets. Finally, the approach outlined here is ready to be applied by the developers of materials sortation equipment so that we can improve the value and purity of recycled plastic waste streams.

Received 19th July 2024
Accepted 13th September 2024

DOI: 10.1039/d4dd00235k
rsc.li/digitaldiscovery

1 Introduction

Polyolefins (PO) are widely used in many areas, from automotive parts to single use plastics and beyond.^{1–3} The subset of plastics made from polymerizing simple olefins/alkenes, POs have a general formula of $(\text{CH}_2\text{CHR})_n$, where R is a simple alkyl group, see Fig. S1[‡] for examples.^{4,5} Academic and industrial research has engineered a wide variety of material properties by varying PO molecular architecture, *i.e.*, the frequency, length, and connectivity of side chain branches off the backbone. These differences in architecture affect how the long molecular

structures interact with one another, in turn affecting their bulk properties such as crystallinity, rheology, and toughness.^{1,2,6} High-density polyethylene (HDPE) is characterized by a linear carbon backbone, with minimal branching. Polypropylene (PP) also displays a consistent backbone, but the propylene monomer results in a methyl pendant on every other backbone carbon. This methyl pendant introduces stereochemistry, however most commercial PP is isotactic.⁷ Low-density polyethylene (LDPE) is constructed with a long carbon backbone, but can vary widely in both the length and frequency of its side chains.¹ If the side chains are consistently short (≤ 6 carbons), then the PO is considered to be linear low-density polyethylene (LLDPE).^{1,8–11} Medium density polyethylene (MDPE) may also be used as a label for samples exhibiting a density somewhere between HDPE and LDPE. Each of these architectures provides a range of mechanical and physical properties, such as improved processability, toughness, durability, tensile strength, opacity, or melting temperature.^{1,12,13}

[†]Materials Science and Engineering Division, National Institute of Standards and Technology, Gaithersburg, MD 20899, USA. E-mail: tyler.martin@nist.gov

[‡]NIST Center for Neutron Research, National Institute of Standards and Technology, Gaithersburg, MD, 20899, USA

[†] Official contribution of the National Institute of Standards and Technology; not subject to copyright in the United States.

[‡] Electronic supplementary information (ESI) available. See DOI: <https://doi.org/10.1039/d4dd00235k>



While this flexibility in POs has been industrially and societally transformative, their widespread use has introduced additional challenges, including environmental impacts.^{14,15} Unfortunately, incompatibility in mixed PO materials drastically impedes recycling and reuse efforts (e.g., multilayer films containing multiple PO species, additives, or poor separation techniques can lead to processing issues, poor mechanical properties, poor appearance, and phase separation in recycled parts).^{15,16} Given that industrial users of post consumer resins (PCR) are looking to avoid such challenges, efficient sorting of POs would enable materials recycling facilities (MRFs) and secondary recyclers to sell more reliable material feedstocks for resin manufacturers, leading to more reliable PCR. The higher the purity of the recycled material, the more valuable it is to users due to a promise of consistent processability. However, when dealing with post-consumer waste, the myriad of shapes, sizes, colors, and other additives can inhibit sortation. Technologies such as recycling codes, near-infrared radiation (NIR), and hyperspectral imaging (HSI) have been developed to help both humans and machines separate various types of plastics, such as polystyrene (PS), polyethylene terephthalate (PET), and POs. While beneficial for speeding up sortation, both simple recycling codes and NIR/HSI technologies have fallen short of enabling rapid and accurate sortation of PO species. Recycling codes are not present on all items, and can be difficult for both machines and humans to find and read, limiting their speed enhancement. NIR and HSI can be employed rapidly, but they struggle to distinguish the various grades of PE from one another, due to the similarity of their vibrational spectra.^{17–22}

To enable better plastic sorting, there is a great deal of literature using analytical chemistry, chemometrics, and machine learning (ML) to provide rapid answers to the identity of any given plastic that may show up on a post-consumer conveyor belt.^{17–23} Using mid-IR (MIR),²¹ NIR,^{22,23} and NIR-based HSI,^{17,19,20} previous research has explored a wide variety of signal correction, normalization, signal smoothing, and differentiation processes to enable their classification techniques to apply to a broader range of samples.^{20–23} These techniques have included the standard normal variate method, mean centering, and detrending for scattering correction, as well as smoothing and differentiation techniques such as the Savitzky–Golay filter. Additionally, various forms of normalization and scaling approaches have been used to better represent the data to ML algorithms. All of these techniques seek to “clean” the data, removing various forms of noise and instrument artifacts from the signal or focusing data analysis on signal derivatives rather than the signal itself. Many of these techniques show promise for enabling ML algorithms to distinguish between polymer spectra, but no consensus exists for when a given method should be used.

Additionally, many of the ML techniques have focused on dimensionality reduction through compared ratios of selected NIR peaks,²² principal component analysis (PCA) of NIR or MIR signals,^{19–21,23} or partial least squares discriminant analysis (PLS-DA) of NIR or MIR signals.^{18,19,21,23} Other techniques have included classifiers such as the soft independent modelling by class analogy (SIMCA),^{20,21} support vector machines (SVM), *k*-

nearest neighbors (KNN), random forest (RF), linear discriminant analysis (LDA), and multilayer perceptrons (MLP).²¹ These models have generally been successful in discriminating between chemically dissimilar materials such as PS, PET, PP, polyethylenes (PE), and polyamides (PA).^{17–23} However, when it comes to classifying the subclasses of POs, these techniques have stopped at differentiating PP from PE, generally failing or not attempting to sort HDPE from LDPE.^{17–20,22} This failure to sort PEs likely stems from the fact that the major spectroscopically detectable difference between POs is the ratio of methyl, methylene, and methine stretches. PP has numerous methine and methyl groups that may distinguish it from PE, but LDPE and LLDPE have far fewer of these pendants, making it likely those vibrations are largely hidden by the vibrations of the methylene groups. A notable exception is the work of Rani *et al.*, where they reported using urban plastic waste and distinguished HDPE from LDPE with perfect accuracy using PLS-DA. However, their PLS-DA model required additional training on just the PE materials, and that work excluded black colored polymers.²³ Additional research is also necessary to consider LLDPE, MDPE, and various form factors such as pellets, flake, or powders (something that may become more relevant with the increase in powder-based additive manufacturing techniques). These form factors can alter the spectra by selectively reflecting different wavelengths depending on the relative size scales of grains or textures.^{24,25}

Here we aim to expand upon previous work to overcome these challenges in recycling POs, using a data-driven approach. Given the diverse methods and plethora of possible combinations that may be applied to analyzing and differentiating these polymers, the current work is intended to act as a resource for understanding many of the preprocessing and machine learning techniques used in plastic classification pipelines. Additionally, this work seeks to provide a benchmarking data set and series of recommended analysis steps to produce rapid, effective, and broadly applicable classification pipelines. We outline a step-wise, reasoned approach to down selection of the computationally intractable number of combinations of preprocessing pipelines, classifiers, and hyperparameters. To accomplish this goal, we first outline our overall approach, then provide brief descriptions of the techniques used at each step of our analysis. Next, this work builds on a previously published National Institute of Standards and Technology (NIST) data set,²⁶ approximately doubling the number of POs to include powders, colored materials, and additional post-consumer resins and uses this data set to evaluate over 12 000 classification pipelines. This set of pipelines is then carefully down selected to identify a single hyperparameter-tuned pipeline that can be reproduced and implemented by other researchers to benchmark their models and processes.

2 Machine learning pipeline components

An overview of our process is represented in Fig. 1 and described as follows. First (Fig. 1a), the expanded data set was



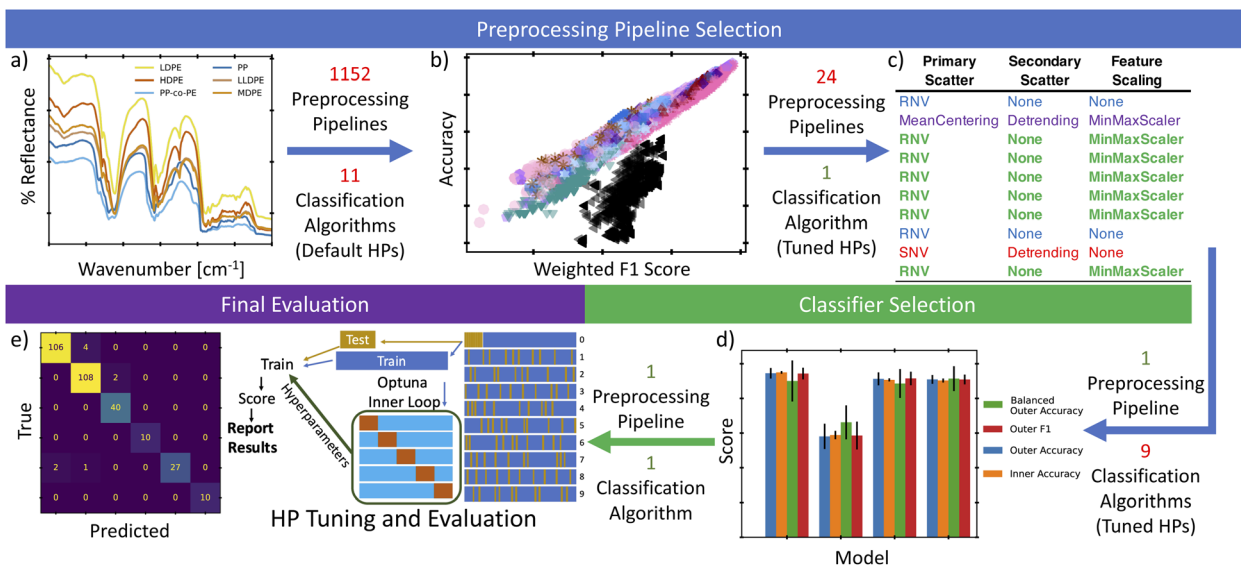


Fig. 1 An overview of our analysis, with original figure and table numbers listed after each step. (a) Initial NIR data was collected from a variety of polymers. Then 1152 combinations of common preprocessing steps were used to correct/transform the data (expanded in Fig. 2). (b) Each of these was then fed into 11 different classification algorithms, using default parameters, and the accuracy and F1 scores were compared (Fig. 3). Based on the top scoring models, the 1152 preprocessing combinations were reduced to a set of 24 combinations that were assumed to produce consistent results (expanded in Fig. 4). (c) These 24 combinations were then evaluated with a nested CV technique and a random forest classification algorithm that could be readily tuned using the Optuna package (expanded in Table 3). (d) The most consistently high-scoring preprocessing combination was then selected for use in another nested CV loop to select the best of 9 Classifiers that could be readily tuned with Optuna (expanded in Fig. 5). (e) Finally, the selected preprocessing combination and the selected classifier were evaluated using a leave-one-group-out adaptation of the nested-CV approach and the corresponding confusion matrix (expanded in Fig. 7).

preprocessed using 1152 combinations of scattering corrections, smoothing, differentiation, normalization, and dimensionality reduction steps. The output of each of these preprocessing pipelines was used to train and test 11 different classification algorithms with default hyperparameters to assess both the benefit of certain preprocessing steps and the ability of each classifier to consistently provide accurate classifications. While simultaneous cross-validation (CV) and hyperparameter tuning on all 12 672 full models (preprocessing pipelines + classifiers) considered in this study would be ideal, it was not computationally tractable in a reasonable timeframe. Instead, we carry out several, partial optimizations that allow us to reduce the size of the search space before applying full cross-validated optimization and tuning. This began with analyzing the scores of these default classifiers to down select the preprocessing steps, Fig. 1b. Next, the best performing preprocessing steps were used with a nested cross-validation (nested-CV) approach to tune hyperparameters of a random forest classifier (RFC). The RFC was trained and tested to enable selection of the most consistently high scoring pipeline for converting a raw NIR signal to a reliable label (Fig. 1c). Based on the result of the nested-CV-RFC study, the most consistent preprocessing pipeline was then used with another nested-CV to tune hyperparameters, train, and test 9 classification algorithms (Fig. 1d). This identified the most consistent and best performing classification algorithm for our data. Next, the selected preprocessing steps and classifier were evaluated using another nested-CV, this time using a leave-one-group-out CV (logoCV) to both tune the hyperparameters and evaluate the

ability of the classifier to classify individual resins that it has not been trained on. Finally, using the hyperparameters suggested from the logoCV, the model was trained and evaluated with a 10-fold stratified shuffle split. The predictions from each split were then concatenated to produce an overview confusion matrix to identify any potential trends in model inaccuracies (Fig. 1e).

2.1 Preprocessing

Preprocessing steps are those performed before the data are given to the ML algorithms. Generally, these steps are meant to remove signal artifacts and noise while also massaging the data so that it is in an ideal form for a given ML algorithm.

2.1.1 Scattering corrections. Polymer films, powders, and pellets scatter NIR light differently, necessitating corrections to remove the effects of sample shape on the collected spectra. Common methods for this include Multiplicative Scattering Correction (MSC), enhanced MSC (eMSC), Standard Normal Variate (SNV), and Robust Normal Variate (RNV).²⁵ MSC and eMSC both require the use of a “scatter-free” reference spectrum to remove scattering artifacts.²⁵ While these methods are useful for analyzing a known sample, they are problematic for use with both unknowns and machine learning algorithms. Not only does one need a reference spectrum, or multiple samples to make a reference spectrum, but the use of this reference greatly increases the chances of data leakage in a machine learning algorithm as information from the reference spectra inherently connects each set of samples to one another. For this

reason, MSC and eMSC are omitted from this work. The Standard Normal Variate uses the mean signal intensity (μ) and the standard deviation (σ) of each spectrum (X_i) to baseline correct and scale the spectra, as shown in eqn (1).²⁵ Theoretically, this allows similar samples to be baseline corrected and scaled similarly, while avoiding a reference spectrum. RNV is based off SNV but seeks to resolve issues that arise from outlier intensity peaks by eliminating potential outliers before determining the mean and standard deviation. Potential outliers are removed by setting a threshold based on percentiles. All data outside of the threshold value(s) is ignored when calculating the mean and standard deviation.²⁷ While the original publication of RNV suggests adjusting the percentile for a given data set, and only omitting high intensities, this work uses the interquartile range (IQR) method described by Rinnan, van den Berg, and Engelsen.²⁵ The IQR form of the RNV corrections uses the data points that fall between the 25th and 75th percentile of a spectra's intensities to identify the effective mean and standard deviation. This is then used to baseline correct and scale the spectrum.

$$X_{i,\text{corr}} = \frac{X_{i,\text{orig}} - \mu_i}{\sigma_i} \quad (1)$$

2.1.2 Detrending and mean centering. Detrending (DT) is another method used to enable scattering correction and is often used alongside SNV.^{25,28} Generally, this method involves fitting a linear best-fit line to the spectra and then subtracting that line from the data to remove any systematic change in signal due to wavelength. Mean centering (MC) takes a simpler approach and subtracts just the mean of the data to zero-center it. This may help reduce collinearity for some models, and is also commonly applied before dimensionality reduction techniques such as PCA.^{25,28,29}

2.1.3 Savitzky–Golay filtering. Savitzky–Golay (SG) filtering is a functional method that uses a sliding window technique to fit a series of polynomial functions to the data.^{30,31} The result is a smoothed version of the data that can also be easily differentiated, enabling analysis of signal derivatives. SG filtering is especially useful for limiting signal noise and for enabling peak location analysis. Previous research has provided mixed reviews on the benefit of this smoothing and differentiation.^{8,20,21,23}

2.1.4 Sample normalization. Normalization to known peaks or total intensities for a given spectrum is a common method in many types of spectroscopy. Some studies have normalized sample spectra by the L1, L2, or area norms.²⁰ While potentially useful for differentiated spectra, it is largely redundant for spectra that have already been scatter corrected using MSC, eMSC, SNV, or RNV, since each of those methods scales the data already.

2.1.5 Feature normalization. Feature normalization is a common machine learning technique used to provide equal weighting to each feature. Unlike sample normalization, this normalization is performed for each wavenumber across all samples. Two of the most common scaling techniques include min–max scaling, and the standard-scaler approach, both of which are included in the Python package scikit-learn.³² Min–

max scaling can be described by eqn (2) where X is a matrix of n samples and m features, X_{\min} is a vector of column-wise minimums ($1 \times m$), X_{\max} is a vector of column-wise maximums ($1 \times m$) and A and B are the minimum and maximum of the desired scale (0 and 1 by default).³³ This scales all data to be between A and B. The standard-scaler is the equivalent of SNV (eqn (1)), but applied for each wavenumber instead of each sample.

$$X_{\text{scaled}} = \frac{X - X_{\min}}{X_{\max} - X_{\min}} \cdot (B - A) + A \quad (2)$$

2.1.6 Dimensionality reduction. Dimensionality reduction is another common machine learning technique, often used to help visualization of complex data. Principal component analysis (PCA), a common version of this technique used in exploratory data analysis, has been especially useful in the NIR research space.^{20,34,35} PCA maps high-dimensional data based on the variance of the features, creating new orthonormal vectors (loadings) that allow comparison of latent variables, also known as PCA scores, rather than entire spectra. Using PCA, it is often possible to visualize differences in NIR with only 2 or 3 dimensions. Functional PCA (fPCA) is an equivalent technique to PCA, but uses functions rather than vectors to represent the new dimensions. While traditional PCA is far more common than fPCA, the functional basis provides a potential avenue to adapt analysis pipelines to data with varying instrument resolutions. In both cases, PCA uses linear mapping to reduce dimensionality, preserving the relative distances between all points in the data set.³⁶ An alternative to these linear methods is non-linear techniques such as Uniform Manifold Approximation and Projection (UMAP).³⁶ Instead of using linear mapping, UMAP uses a manifold learning techniques to construct a topological representation of the data and then optimizes the layout of the data in the new low-dimension space, while attempting to preserve local, relative distances between data points.³⁶ This may be better suited for many types of data that have various scales of variation and benefit from preservation of local distances rather than global distances.³⁶

In terms of data visualization, a noteworthy weakness of both PCA and UMAP as described, is that they are unsupervised techniques, meaning that the new dimensions they construct separate the data itself, not the classes or labels we may actually want to sort. This means that samples with varying form factors, thermal history, or additives may be separated more effectively than those of different PO classes. When attempting to visualize data differences, it may be more beneficial to use techniques such as a supervised version of UMAP, or the latent variables that are created during some classification algorithms such as PLS-DA, linear discriminant analysis (LDA), and quadratic discriminant analysis (QDA). These techniques use the data labels (polymer class) to reduce the data in a way that maximizes the separation between classes, rather than every data point. However, supervised dimensionality reduction should only be used with great care. If the real-world variety is not sufficiently represented by the training data, it greatly increases the chances



of overfitting the model to the training data and providing overly optimistic scores when compared to real-world testing.

2.2 Classification algorithms

Once the data are properly preprocessed, it is fed into a classification algorithm as training and testing data sets. A brief description of the supervised algorithms used in this paper is provided below to help the reader understand the differences in the methods. This includes every classification algorithm in the scikit-learn documentation at the time of writing, with the addition of some field-specific models. For reference, the features are the wavenumbers that correspond with the collected NIR intensities.

2.2.1 Discriminant analysis. Discriminant analysis is a technique that relies on dimensionality reduction to create a mapping of the samples that enables a line to be drawn between data classes. Here we present three of the most commonly used algorithms. In many cases, this involves a dimensionality reduction step, similar to those mentioned in 2.1.6, however, a key difference is that discriminant analysis techniques are supervised, meaning they reduce dimensionality in emphasizes variation between target classes rather than differences between all spectra.

2.2.1.1 Partial least squares-discriminant analysis (PLS-DA). PLS-DA is one of the most commonly used discriminant techniques, but it relies on regression-based prediction of labels, leading to much confusion throughout the literature.^{37,38} The algorithm takes an m by n data array (\mathbf{X}) and a “label” array of m by l numerical or binary labels (\mathbf{Y} , or y if $l = 1$), where m is the number of samples, n is the number of features, and l is either the number of labels or the number of labels minus one. For additional clarity, a sample labeled as HDPE may be represented in \mathbf{Y} as $[1, 0, 0]$ to indicate that it is labeled as HDPE, but not labeled as LDPE or LLDPE. A regression model is then performed between \mathbf{X} and \mathbf{Y} , to enable prediction of a number between 0 and 1 for each column/variable of \mathbf{Y} . During this process, latent space components consisting of loadings and scores are created, such that the weighting vector maximizes covariance between the two arrays. Similar to PCA, the latent variables are constructed such that the first loading vector accounts for the most variation, and subsequent vectors are created from the using the residuals of the prior latent variable for \mathbf{X} and \mathbf{Y} .³⁹ The number of components used in the final prediction can be down selected, where more components describe the data more fully but can also increase the chance of overfitting. It is important to again note that PLS-DA is not a true classification technique, it is a regression technique providing a coefficient vector that can be used to predict an unknown sample's label (in-class or not in-class). Since this is regression-based, the predicted label requires some level of post-prediction decision boundary to convert the prediction to a class label. In the case of \mathbf{Y} composed of binary labels (0/false or 1/true for each label), the algorithm must convert decimals between 0 and 1 to a set of class labels. This means a sample's true label may be $[0, 1, 0]$ but may have a predicted label of $[0.1, 0.7, 0.2]$ or $[0.5, 0.5, 0.5]$. These decimals then must be rectified

to produce a final label such as HDPE, LDPE, or LLDPE. It should be noted that each prediction coefficient is effectively unrelated to one another, meaning $[0.1, 0.7, 0.2]$ does not represent a blend of polymers nor anything similarly percentage based. They are independent numerical values to represent where a given sample falls relative to the extremes of in-class (1) and not in-class (0), for each possible class label. A simple method to rectify these vectors into a single label is to round values to the nearest integer, but this may cause issues for samples labeled similarly to $[0.5, 0.5, 0.5]$, as a sample is unlikely to be in all three categories at once. In the scikit-learn distribution, there are two types of PLS-DA.³³ PLS1-DA is designed to handle a dichotomy of classes (\mathbf{y}), while PLS2-DA is designed to handle multiple classes (\mathbf{Y}). PLS1-DA can still be used with multiple classes, but generally requires multiple PLS1-DA classifiers to be trained in a one-vs.-rest manner. This further complicates analysis, as additional rules must be made to rectify the multiple classifiers into a single prediction. PLS2-DA is capable of predicting multiple outputs with the previously mentioned series of in-class *versus* not in-class comparisons. This creates a new regression for each label, increasing flexibility. However, it faces issues with the weighting of \mathbf{X} , potentially penalizing larger groups if the labels are not equally distributed across samples.³⁷ To combat this, the \mathbf{X} can be weighted for each variable of \mathbf{Y} , but this can be complicated to implement.³⁷ For a more in-depth understanding of PLS-DA, readers are directed to ref. 37, 38 and 40.

2.2.1.2 Linear discriminant analysis (LDA). LDA functions similarly to PLS-DA such that PLS-DA using all latent variables should provide the same decision function as LDA, at least for a 2-class system.⁴¹ However, LDA measures distances using the Mahalanobis distance instead of the Euclidean distance.³⁷ During this calculation, a single covariance matrix is generated to describe the variance of each class with respect to its features. With this technique, LDA is more readily able to handle features that may be of widely different scales as well as multi-class problems.³⁷ However, despite these advantages, the decision boundary that LDA provides is still linear, meaning that it may not provide good results for class separation if the classes are not linearly separable.³³

2.2.1.3 Quadratic discriminant analysis (QDA). To combat challenges with non-linearly separable data, QDA offers a more flexible decision boundary. Instead of applying a linear decision boundary to discriminate between classes, QDA uses a quadratic function. This is made possible by applying a different covariance matrix to each class, rather than one matrix that effectively averages the covariance across classes.⁴² While this may be more computationally expensive, it yields much more flexibility for data that may not be linearly separable.

2.2.2 Support vector machines/support vector classifiers (SVM/SVC). Rather than reducing dimensionality, SVM models take advantage of high-dimensional space to draw a hyperplane between the data points of two classes.⁴³ The hyperplane is drawn such that it maximizes the distance between the hyperplane and the outer data points of each class. The algorithm uses various weighting functions to enable better separations of



the data.⁴⁴ While generally designed for binary classification problems, SVMs can be used in multi-class problems. Instead of using a one-vs.-rest approach as mentioned with PLS-DA, SVM often uses a one-vs.-one approach. This method effectively creates multiple SVM models that separate one pair of classes at a time *i.e.* (1) – HDPE *vs.* LDPE, (2) – HDPE *vs.* LLDPE, (3) – HDPE *vs.* PP, (4) – LDPE *vs.* LLDPE, (5) – LDPE *vs.* PP, *etc.* When predicting the class of a data point, models “vote” on the class, *i.e.* for the preceding example of 5 one-vs.-one SVMs, the SVMs may classify a sample as (1) – HDPE, (2) – HDPE, (3) – HDPE, (4) – LDPE, and (5) – LDPE, respectively leading to an overall HDPE prediction. SVMs can be tuned to use various kernels to generate the hyperplane, the simplest of these is a linear kernel (LinearSVC), and the most common of which is the radial basis function (RBF) or Gaussian kernel. SVMs may also be used for regression problems, and thus classification SVMs are often referred to as Support Vector Classifiers (SVCs).

2.2.3 Soft independent modelling by class analogy (SIMCA). SIMCA is commonly used in chemometric literature, especially when “soft” classifications, or nonexclusive labels are needed.^{20,45,46} Developed by Wold and Sjöström in 1977, this technique uses PCA to transform each class into a class-PCA space. When new (unknown) samples are introduced, they are transformed into each of the PCA spaces and an average orthogonal or Euclidean distance is calculated to describe how far the new sample is from the center of the class.^{45–47} If this distance is less than a user-defined critical distance, the sample is considered part of that class. If the distance is greater than the critical distance, the sample is marked as not part of that class. Each sample can be labeled as belonging to anywhere from none to every class. This can be advantageous for situations where there may be significant overlap between samples, such as subclasses of polymers, however training and interpretation of the model can quickly get complex with additional classes. Recently, concerns about the quality of this method have surfaced, favoring discriminant analysis techniques such as PLS-DA and QDA.^{45,46}

2.2.4 *k*-Nearest neighbors (KNN). KNN is one of the simplest voting classifiers. Using labeled data, KNN determines the distance between a new data point and the *k*-nearest data points. The most common label is then used for the new data point. The number of neighbors (*k*) can be easily adjusted, and is commonly tuned to balance bias and accuracy. Additionally, it is possible to weight each neighbor's vote based on how close they are to the unknown data point.³³

2.2.5 Gaussian naive Bayes (GNB). Naive Bayes algorithms are conditional probability-based models that make the “naive” assumption that there is no interdependence between the various features.^{33,48} In the case of GNB, it is also assumed that the response for each feature is normally distributed across a class. This is to say that each class has an expected distribution of values for each feature. Predictions are then made using the likelihood that a new data point would fall into a class's distribution given its set of feature-value pairs.⁴⁸ While not necessary, Naive Bayes algorithms can be given prior probabilities to describe the probability that a sample is in a given class. For example, if a secondary recycler is sorting a bale of recycled

plastic from an MRF labeled as “>95% polypropylene” the GNB can be biased to assume any unknown sample is most likely PP. This way, one can use prior knowledge to help decide predicted labels when the results might otherwise be ambiguous.³³ If this information is not provided as an argument during initial model training, the class probabilities will be learned based on the supplied training data. Therefore, if priors are not supplied, the ratio of classes of the training data should match the real-world ratios as closely as possible.

2.2.6 Multilayer perceptron classifier (MLPC). MLPs, or Artificial Neural Networks, are a form of machine learning model designed to mimic how biological neurons communicate. Biological neurons are connected to many other neurons as both inputs and outputs, and the pattern of connections that are triggered by an initial stimulus leads to a final output. For MLPs, a perceptron is analogous to a neuron, and the model is made of multiple layers of perceptrons. For a given layer, the perceptron takes input from every perceptron from the layer before it, and provides a weighted and biased output to every perceptron in the next layer after it. Generally speaking, the first layer will reflect the size of the data, while the last layer will reflect the size of the desired output. The layers in between will step down the initial inputs, using weighting and biasing to determine the value of the signals passing between each perceptron pair to determine how strongly the following perceptron should be activated. Training MLPs involves tuning the weights, biases, and the structure of the middle layers to ensure activation of the ideal final perceptron/label.^{21,49}

2.2.7 Decision trees. Decision tree classifiers are built by repeatedly splitting the data into one of two nodes,⁵⁰ which can be thought of as repeated binary classification. Starting at the initial node or root, the algorithm uses a single feature to split the data into two nodes or branches. Each branch can then split again, creating another level of the tree. When a node no longer splits, it is known as a leaf, and should provide the final class label. In most algorithms, trees can be tuned to only have a certain number of branches or levels, or to ensure that each leaf contains a given number of samples. These tuning parameters may hurt the initial accuracy of the classification, but allow the decision tree to handle new data better (avoiding overfitting). New samples are brought through the decision tree, following the path that matches the features of that data (*i.e.* taking the $x_1 < 0.5$ branch for a sample with $x_1 = 0.25$).⁵⁰

2.2.7.1 Random forest (RF). RF classifiers rely on an ensemble of decision trees to vote on the correct label. Multiple trees are created simultaneously with different sets of sample data and with different splitting decisions. When a new sample is introduced, it is classified by each tree and the class with the most votes is returned as the final class prediction. The size and shape of the individual trees can be controlled, as well as the number of trees used to create the forest.³³

2.2.7.2 AdaBoost. AdaBoost classifiers function similarly to RFs, but generate new decision trees using information from the previous trees. As new trees are created, weights are introduced to penalize inaccurate classifications and to focus training on avoiding such errors. The result is a forest of trees that have weighted votes when predicting new sample labels.



Trees that performed poorly will have less weight to their vote than trees that performed well. Additionally, AdaBoost traditionally uses decision “stumps” instead of decision trees, meaning that each tree only splits the data once.³³ While tuneable, this default tree size can play a large role in both the speed and accuracy of the final model.

2.3 Code specifications

2.3.1 Preprocessing. Unless noted otherwise, all preprocessing techniques were employed as described in Section 2.1. The mean centering step subtracted the mean intensity from all intensities across wavelengths. The RNV step used the IQR method for limiting outliers. The detrending and Savitzky-Golay steps used the detrend and savgol_filter functions (respectively) from `scipy.signal 1.12.0`.⁵¹ Savitzky-Golay filtering used window length of 21 and polynomial order of six based on the quality of fit and ability to remove noise without adding distortions. Further explanation of the methods used to determine these parameters can be found in the example Jupyter notebooks provided in the associated GitHub repository ([usnistgov/ECAPS](https://github.com/usnistgov/ECAPS)).²⁶ Additionally, the Savitzky-Golay function used a delta of approximately 1.928, the average spacing between our wavelength resolution. The sample and feature normalization steps used the Normalizer, MinMaxScaler and StandardScaler transformers from the preprocessing package of `scikit-learn 1.2.0`.³³ PCA was also performed using the `scikit-learn` implementation. `scikit-fda` version 0.9.1 was used for fPCA,⁵² and `UMAP` version 0.5.5 was used for the UMAP dimensionality reduction.³⁶

2.3.2 Classification. All classification algorithms, except for the SIMCA model, were from the `scikit-learn` package, version `1.2.0`.³² The SIMCA model used for this work was adapted from ref. 21, and the modified version is available in our Python code repository ([usnistgov/ECAPS](https://github.com/usnistgov/ECAPS)).²⁶

3 Experimental methods

3.1 Materials

For this study, 31 POs, representing commercial plastic samples (including 11 PCRs), were used along with 9 PO samples from the Hawaii Pacific University Polymer Kit 1.0.⁵³ Additionally, National Institute of Standards and Technology (NIST) PE Standard Reference Materials[®] 1473, 1474 and 1476 were included. This data includes 19 polymers characterized in ref. 26 and 24 new materials. For ML training purposes, supplier labels of PO type were assumed to be accurate labels. A summary of the samples and their sources is provided in Table 1. Table S2‡ contains information on the physical state and presence of color in the samples.

3.2 Near-infrared spectroscopy

NIR measurements were collected on a Nicolet iS50 NIR module, Thermo Fischer Scientific (Waltham, MA), at 4 cm^{-1} resolution and an accumulation of 32 scans with an integrating sphere, a sapphire window, calcium fluoride (CaF_2) beam splitter, a gold internal reference, and an indium gallium

Table 1 Summary of the sample sources used in this study

Source	HDPE	MDPE	LDPE	LLDPE	PP	PP-co-PE
Commercial polymers	12	0	11	3	3	2
Hawaii Pacific University	2	1	3	2	1	0
NIST	1	0	2	0	0	0
Total	15	1	16	5	4	2

arsenide (InGaAs) detector.⁵⁴ Internal background and dark corrections were applied to the measurements. Pellets were used as received and filled at least halfway in a 10 mL or 20 mL VWR borosilicate glass scintillation vial as a representative aliquot of the sample resin. Each sample was measured 7 times, where the vial was shaken between scans in an attempt to redistribute the pellets in the vial and account for local composition variations. The vial was then placed flat on the NIR module, centered above the beam path. Additionally, changes in sample vial and vial lids were confirmed not to alter the reflected NIR signal significantly.

3.3 Data analysis

Data analysis was performed using the Python coding language and freely available open-source packages. The code and the raw data used for this study are made available on the NIST Data Repository and GitHub.⁵⁴ ML cross validation (CV) methods are described in detail in Section 5.

4 Results and discussion

4.1 Preprocessing

To evaluate the myriad of possible preprocessing and classifier combinations, it was necessary to design a systematic approach to test as many combinations of preprocessing steps and classification algorithms as possible. This was accomplished by splitting preprocessing steps into a maximum sequence of 6 functions: basic scatter corrections (mean centering, SNV, RNV), detrending, Savitzky-Golay filtering (and derivatives), spectra normalization (L1 and L2 norms), feature normalization (StandardScaler, MinMaxScaler), and dimensionality reduction (PCA, fPCA, UMAP). With each step of the preprocessing pipeline also having a “no correction” level, this creates a total of 1152 possible preprocessing combinations. A small selection of how these preprocessing techniques affect the data can be seen in the plots of Fig. 2. In this figure, the top row is the “spectra” view, while the bottom row is a reduced visualization using fPCA to demonstrate the potential for separation of the data with those corrections applied. From left to right, it shows the otherwise unprocessed data, the RNV corrected data, and the RNV corrected data with a second-derivative SG filter (SG'') applied. This figure clearly demonstrates how impactful preprocessing can be on the final results of a machine learning algorithm, especially with unsupervised techniques like fPCA. The variation in reduced data stems from the removal of different sources of variation in the provided data, allowing different features/wavenumbers, and trends to stand out.



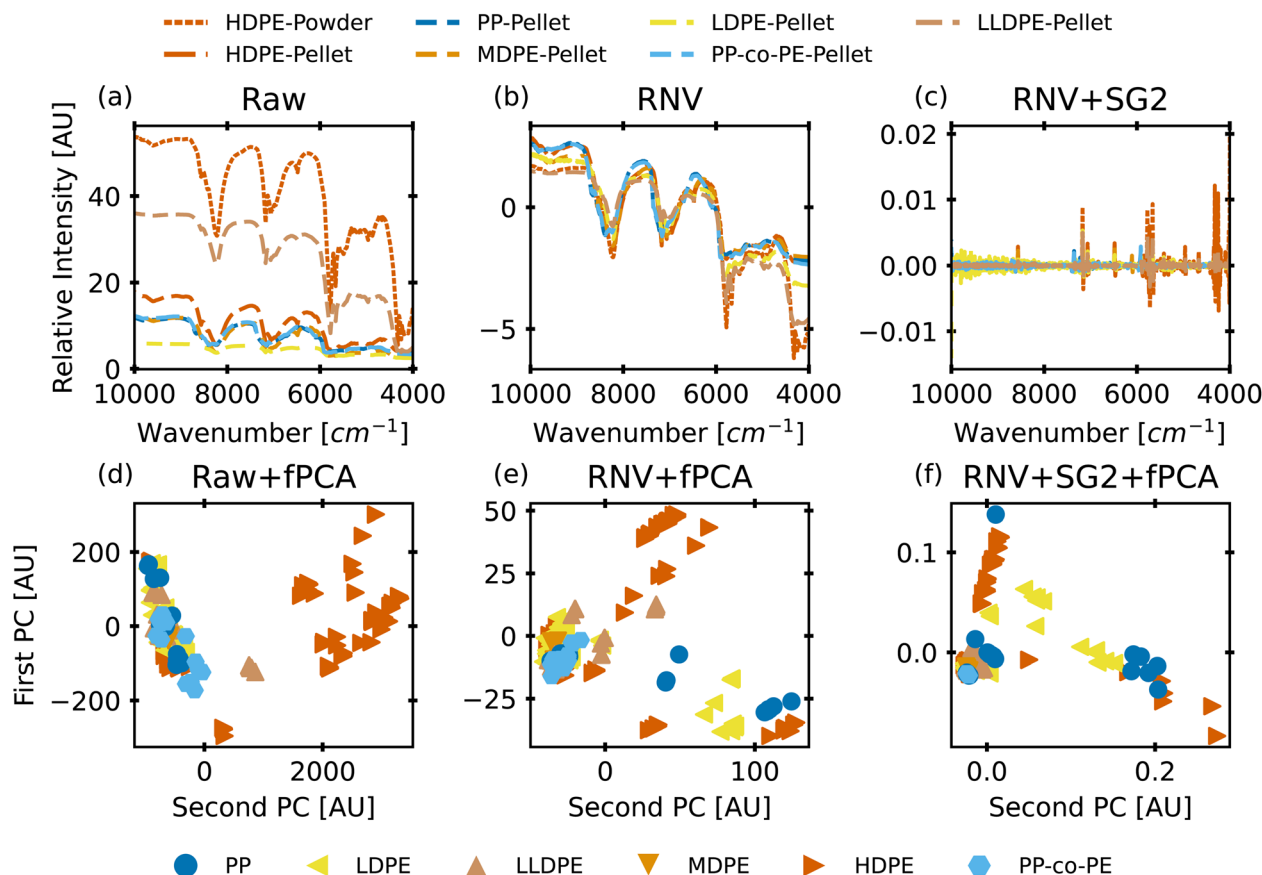


Fig. 2 A comparison of some (a–c) full spectra and (d–f) fPCA scores with (a and d) no other preprocessing, (b and e) RNV corrections, and (c and f) RNV corrections followed by a second-derivative Savitzky–Golay filter. This represents 6 of the 1152 different pipelines, each of which may be provided to the ML models for training and testing. Overlapping samples in both spectra and reduced dimensions demonstrate the difficulty of sorting samples with large amounts of overlap, no matter the preprocessing steps.

4.1.1 Preprocessing pipeline selection. Differing samples, classification questions, and ML algorithms will benefit from different sets of preprocessing steps. This has likely led to the wide variety of techniques and strategies used to sort polymer waste.^{17–23,55} However, it is often useful to have a benchmark for comparing multiple strategies, necessitating the preprocessing step that offers the most consistent success across various algorithms. Therefore, 11 different ML classifiers were trained and tested on each of the 1152 pipelines, producing 12 672 different classification models and corresponding scores.

During this step, each classifier was initiated using predominantly the default parameters, with no hyperparameter tuning. A summary of the parameters that were set to non-default parameters is shown in Table 2, and the default parameters for each model are presented in Tables S3 through S5.‡ These models were then trained and tested using a stratified train-test split, withholding 33% of the data for testing. Classifiers were compared by their accuracy (eqn (3)) and their weighted F1-score (eqn (6)). Accuracy provides a simple metric of how many samples were correctly labeled, while the weighted F1

Table 2 Non-default parameters for the initial classification study using all 1152 preprocessing pipelines. For PLS-DA, the number of components was adjusted to roughly compare changes in accuracy with additional components. MLPC iterations were increased from the defaults to limit convergence issues

Common name	Classifier	Source	Parameters
PLS-DA	PLSRegression	scikit-learn 1.2	<i>n_components</i> = 3
PLS-DA	PLSRegression	scikit-learn 1.2	<i>n_components</i> = 5
MLPC	MLPClassifier	scikit-learn 1.2	<i>max_iter</i> = 2000
SIMCA	SIMCA_classifier	Custom code adapted from ref. 21 and 56	<i>simca_type</i> = 'SIMCA' <i>cat_encoder</i> = OneHotEncoder (**) ** <i>sparse_output</i> = false, ** <i>handle_unknown</i> = 'ignore'



score attempts to add penalties for models that systematically mislabel a class due to limited sample numbers. In these equations, n is the number of samples, y is the vector of true labels, \hat{y} is the vector of predicted labels, $1(x)$ is the indicator function, L is the set of possible labels, y_l is the subset of y with the label l , and \hat{y}_l is the subset of \hat{y} with the label l . The weighted F1-score is a weighted harmonic mean of the precision (eqn (4)) and recall (eqn (5)) scores, thus reducing precision and recall to a single axis. For the scikit-learn implementation of eqn (4) and (5), if the denominators are 0, then P and R are set to 0. For more information on scoring criteria, readers are directed to Section 2.4 of scikit-learn's user guide.³³

$$A(y, \hat{y}) = \frac{1}{n} \sum_{i=0}^{n-1} 1(\hat{y}_i = y_i) \quad (3)$$

$$P(y, \hat{y}) = \frac{|y \cap \hat{y}_l|}{|\hat{y}_l|} \quad (4)$$

$$R(y, \hat{y}) = \frac{|y \cap \hat{y}_l|}{|y_l|} \quad (5)$$

$$wF1(y, \hat{y}) = \frac{1}{\sum_{l \in L} |y_l|} \sum_{l \in L} |y_l| \frac{2 \times P(y_l, \hat{y}_l) \times R(y_l, \hat{y}_l)}{P(y_l, \hat{y}_l) + R(y_l, \hat{y}_l)} \quad (6)$$

Fig. 3 presents the results of this initial study, organizing models by their weighted F1 score and their accuracy. While most models follow a similar linear relationship between their accuracy and F1 score, the SIMCA model differs from the trend. This is most likely due to the “soft” nature of the model, allowing it to give multiple labels to a single sample, where the other algorithms output one label per sample. With the applied accuracy metric, any sample that has multiple labels will automatically be scored as incorrect, since the true label has only one classification. Since SIMCA is largely designed to produce

multi- or “soft” labels, it is understandable that the SIMCA algorithm is systematically penalized with the chosen metric.

An ideal preprocessing pipeline should enable multiple ML models to score highly on both accuracy and F1 tests. Fig. 4 focuses on the models that scored above 90% for both metrics, and highlights them based on which preprocessing steps were used for each stage of the pipeline. The highest accuracy model was preprocessed with RNV, no detrending, no SG filtering, an L1 normalization step, a StandardScaler step, and no dimensionality reduction.

Fig. 4 provides an opportunity to limit the preprocessing steps used with our models through elimination of steps that systematically add computation time without increasing scores. Limiting preprocessing steps or levels of those steps frees up computational power to tune hyperparameters and identify a more robust model. To reduce the available preprocessing steps, a few assumptions were made. Predominantly, if one of the 6 steps did not provide obvious improvement, but did add complexity to the model, we would not use any levels of that step. For example, Savitzky-Golay filtering relies on a set of parameters that can be arbitrarily set, such as window length, polynomial order, and sample spacing. These parameters can drastically change the results of the fit, necessitating a standard method to apply the filter. Since noisy and smoothed samples performed similarly in our tests, this step can be removed. Similarly, we remove the spectra normalization (step 4, lower left) step. Both RNV and SNV already perform some level of spectra normalization, further making this step partially redundant. Dimensionality reduction (step 6, lower right) displayed a marked decrease in performance, so it was also eliminated. Feature scaling (step 5, lower center) was kept, as many models in the scikit-learn package are documented to rely heavily on feature scaling for accurate results.^{33,57} This provides 24 possible pipelines, combinations of steps 1, 2 and 5, which can be used to tune a classification model to identify the most robust preprocessing pipeline.

To further reduce the 24 pipelines down to 1, a random forest model was trained and tuned using a nested-cross validation (CV) approach⁵⁸ and the Optuna Python package.⁵⁹ For

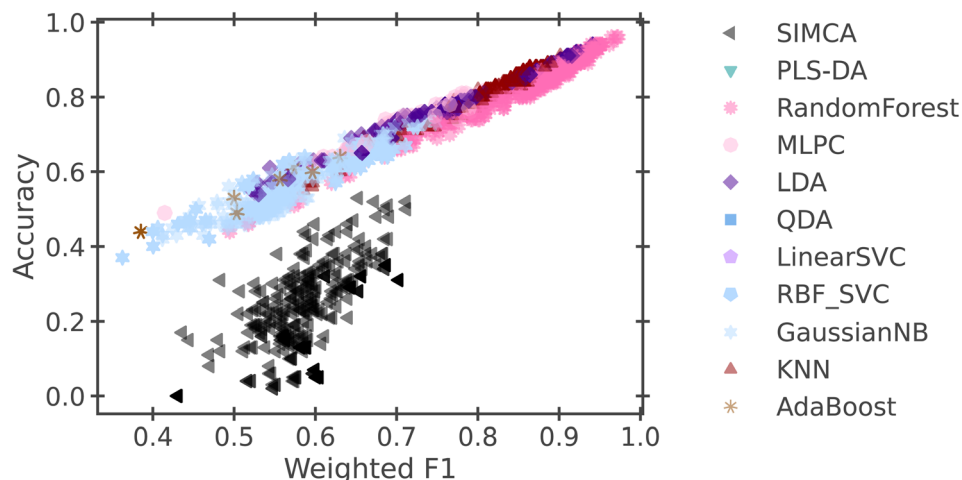


Fig. 3 The accuracy and weighted F1 scores for 12 672 models that were trained with default parameters.



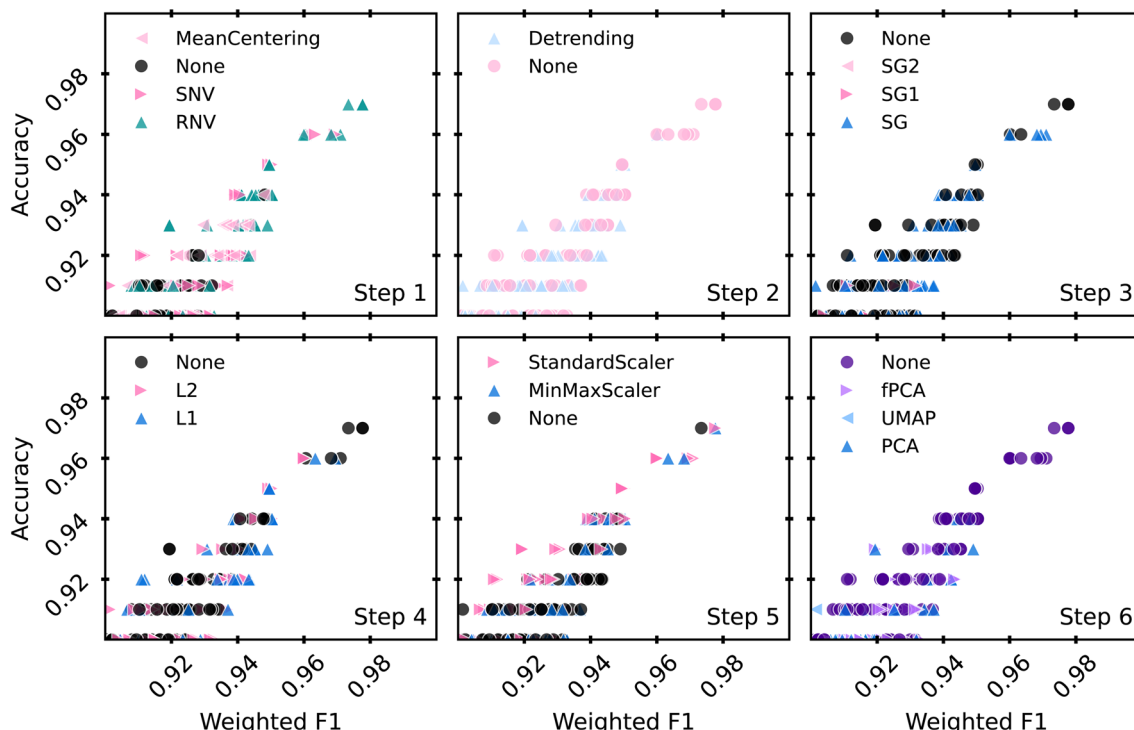


Fig. 4 An alternative view of the high scoring models, including those with warnings. Models are highlighted by their preprocessing technique at each of the 6 preprocessing steps.

this approach, the raw data was preprocessed by each of the 24 preprocessing pipelines, and the Optuna loop was able to select from the pipeline steps while also tuning the random forest model hyperparameters for the selected preprocessing pipeline. In the tuning step, Optuna uses a Tree-structured Parzen Estimator (by default) to rapidly and effectively tune provided hyperparameters of a given model.⁶⁰

The nested-CV used a 10-fold stratified shuffle split as the outer loop, and a 5-fold CV inside the Optuna objective function as the inner loop. The inner loop enables careful tuning of the hyperparameters and preprocessing steps, while the outer loop holds an additional set of testing data that are hidden from every iteration of the inner loop's training steps. For each iteration of the inner loop, the Optuna study used 1000 trials to identify the best set of preprocessing steps and random forest

hyperparameters, based on the mean accuracy of the 5-fold CV score. This set of tuned model parameters and preprocessing steps was then used in the outer loop to train a new RF model on all the data from the inner loop, and tested on data reserved from the initial 10-fold stratified shuffle split. The general workflow for this nested approach can be seen in Fig. 1e. It should be noted that the RF classifier was chosen for this step because it demonstrated a strong distribution of high weighted F1 scores across most of the initial 1152 preprocessing pipelines. The distribution of scores for each classifier is presented as a violin plot in Fig. S2.‡

The results of each outer loop are reported in Table 3. The results of the initial nested-CV show that RNV alone performed the best out of all the iterations. However, it was only selected by the inner loop a single time. In favor of a robust model, RNV

Table 3 Scoring metrics from each of the 10 iterations used to select the most robust preprocessing pipeline. Using RNV and MinMaxScaler provided the best results from the inner loops for 6 of the 10 iterations

Primary scatter	Secondary scatter	Feature scatter	Inner accuracy	Outer accuracy	Outer F1
RNV	None	None	94.8%	100.0%	100.0%
MeanCentering	Detrending	MinMaxScaler	93.3%	87.1%	86.8%
RNV	None	MinMaxScaler	94.8%	96.8%	95.2%
RNV	None	MinMaxScaler	95.2%	93.5%	92.1%
RNV	None	MinMaxScaler	94.4%	93.5%	92.7%
RNV	None	MinMaxScaler	93.7%	93.5%	92.1%
RNV	None	MinMaxScaler	95.6%	93.5%	92.0%
RNV	None	None	95.2%	90.3%	89.1%
SNV	Detrending	None	93.7%	90.3%	88.5%
RNV	None	MinMaxScaler	94.4%	90.3%	88.8%



with a MinMaxScaler (RNV-MMS) step was chosen as the final preprocessing pipeline, since it was selected by the inner loop for 6 of the 10 outer loop iterations. Additionally, since some ML models benefit strongly from feature scaling, the additional MinMaxScaler step should enable those algorithms to perform their best.^{33,57} The RNV-MMS data can now be used to tune a wide variety of scikit-learn classification models.

4.2 Model evaluation

To isolate a single classification model as the best candidate for a benchmark study, we use another nested-CV approach to select the best candidate. Using the selected RNV-MMS pre-processed data, we create a new nested CV that loops through 9 different scikit-learn classifiers, tunes the hyperparameters with an Optuna study, and then evaluates the final results. This process repeats for another 10 iterations, providing mean accuracies and standard deviations for each classifier. It should be noted that both SIMCA and PLS-DA were removed from this analysis. This choice was made due to the additional need for post-model rectification of labels. Additionally, Fig. 3 revealed that both SIMCA and PLS-DA consistently returned some of the lowest accuracy scores. Finally, to ensure that classes with lower sample numbers (MDPE, PP, and PP-*co*-PE) were not consistently misclassified, this analysis began using weighted or balanced accuracy scores along with traditional accuracy. This method adds a weighting factor based on the support (number of samples) for each class. This is to say that providing an incorrect label to a class with fewer samples is more detrimental than providing an incorrect label to a class with more samples. The averaged results of this step are presented in Fig. 5. Most models performed well, with only KNN (89%), GaussianNB (66%), and QDA (52%) having lower than 90% accuracy when adjusted for data set imbalance (balanced accuracy score). LinearSVC held the highest mean balanced-accuracy score (95%) and was selected as the best classifier for this work.

4.3 Leave one group out (LOGO)

While the previous analysis evaluates the strength of LinearSVC to differentiate various types of known POs, it does not address how LinearSVC performs when it needs to categorize a new polymer, such as a new batch of HDPE. One way to test this robustness is to remove one polymer species (all replicates) from the training set, and instead use that polymer to test the model. Repeating this for each polymer species in our data set enables a leave-one-group-out cross validation (LOGO). Fig. 6 demonstrates the results of using a LOGO approach for the inner loop, selecting hyperparameters for the LinearSVC based on LOGO scores. In this version of the nested-CV approach, the data are split normally with a 10-fold stratified shuffle split, then all the replicates of one polymer species are used for the testing set of the inner (Optuna) loop. The outer loop is then used to evaluate if the same hyperparameters can be used to retrain the model with the new data, but without re-tuning the model. Ideally, this reflects the process that would be used by a commercial facility, as re-tuning the model's hyperparameters whenever a new polymer is identified would be much more computationally expensive than retraining the model with the same hyperparameters. For reference, the full LOGO-CV script took approximately 12 hours to run and optimize hyperparameters on a Windows desktop computer equipped with an Intel Core i7 13700KF processor and 32 GB of 5600 MHz DDR5 RAM.⁵⁴ However, training on 90% of our data set, with the optimized hyperparameters completed in under 4 seconds, and predictions of the remaining 10% testing set were complete in under 1 ms.

The inner accuracy score reflects how poorly the model can classify these “unknown” samples, averaging approximately 60% success across the loops. However, given the imbalance in this data set, the 60% may be surprisingly accurate when considering that the MDPE category only has 1 polymer species, and the PP-*co*-PE only has 2 species. This means that when the

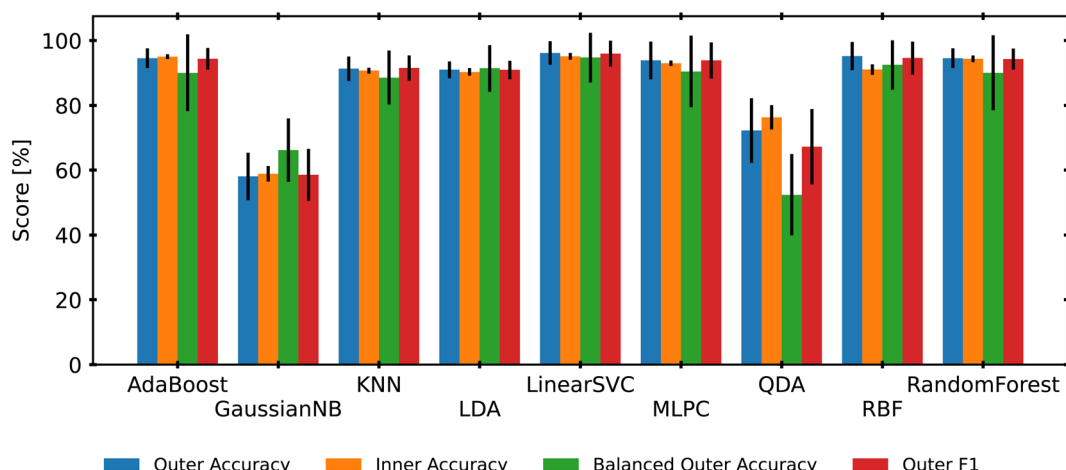


Fig. 5 A bar plot of the mean and standard deviation of model scores for each Optuna tuned classifier. The inner accuracy is the average 5-fold CV score from all 1000 Optuna trials. AdaBoost and RandomForest represent the decision tree-based classifiers, GaussianNB is the Gaussian Naive Bayes algorithm, KNN is *k*-nearest neighbors, LDA and QDA are the linear and quadratic discriminant analysis techniques, LinearSVC and RBF are both support vector machines with different kernels, and MLPC is the multilayer perceptron classifier.



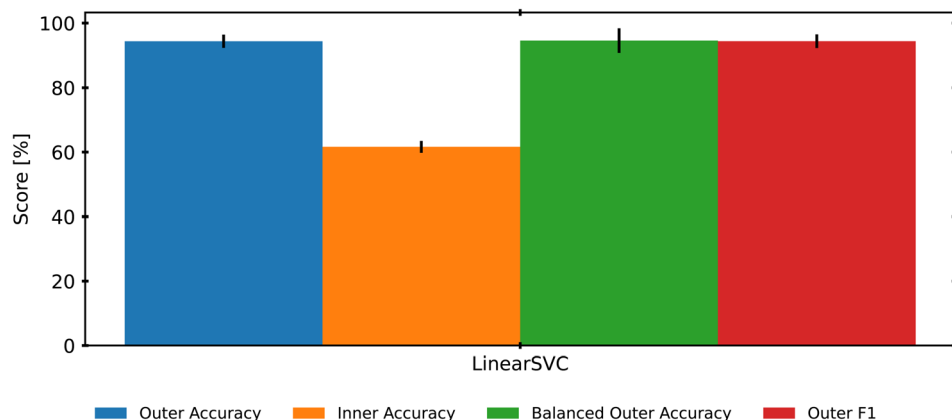


Fig. 6 Using a leave one group out CV approach during the Optuna scoring procedure leads to low inner loop scores, but may produce a set of final hyperparameters that lead to a more robust final model.

single MDPE polymer is removed, there is no MDPE data to train the LinearSVC on. This guarantees complete failure when the model is asked to classify the MDPE polymer that has been held out – the model will not know the MDPE class at all but will be expected to correctly label the 7 MDPE samples as MDPE. Similarly, the PP-*co*-PE samples vary significantly since they are copolymers, and having only one example of a copolymer in the data set likely hampers the test results. While these sample-limited classes could be removed to improve results, retaining them reflects the potential for novel materials and the potential impact on an industrial facility. Despite this challenge, when the resultant hyperparameters are used to retrain the model on all polymer species, the LinearSVC performs with 95% accuracy again.

This finding is particularly promising given that there is much research on innovative chemistries that are producing new polymers and new mixtures of polymers. When a recycling facility identifies a new polymer that may be causing issues in the sorting process, they will likely need to retrain their sorting model to identify the new polymer. However, retraining a model on new data is much quicker if the hyperparameters can remain the same.

4.4 Final model analysis

For the final analysis, we average the hyperparameter values chosen by the 10 iterations of Optuna trained *via* LOGO to suggest a generalized model that can be employed without the tuning step. For LinearSVC the hyperparameters are as follows.³³ *C* is the regularization parameter, meant to scale the loss function with relation to the penalty term. *penalty* is the penalty term that penalizes the optimization function for misclassifying a sample. *multi_class* determines if the SVC algorithm uses a one-vs.-rest approach to generate one SVC per class or tries to create one SVC that tries to separate all classes at once. *class_weight* enables adjusting *C* for each class, based on class size. *max_iter* limits how many iterations the models used to optimize the support vectors before it is forced to stop. *dual* determines what level of optimization the model uses. *tol* is the

tolerance level for misclassification errors. The values obtained from both the initial nested-CV and the LOGO nested-CV can be seen in Table 4. The values for *C* and *tol* were taken as the mean from the 10 iterations. The *max_iter* argument was increased to 10 000 to guarantee convergence of the model, and all other arguments were the mode of the 10 iterations.

For a final evaluation of this model we conduct a 10-fold cross validation, using the *StratifiedShuffleSplit* method of scikit-learn. With a training set of 10% of the total data for each shuffle, we obtained an average weighted accuracy score of 98%. The confusion matrix generated from the cross validation study is presented in Fig. 7. The confusion matrix enables a view into where the final model struggles. Despite the limited amount of PP, PP-*co*-PE, and MDPE samples, we see only one misclassification from all the 10 iterations. Such a success with samples that have only had minimal support during training is likely due to the emphasis on a weighted or balanced accuracy metric. These metrics limit a model's incentive to "cover-up" failures by classifying questionable samples as the majority class. Instead, the errors lie with the majority classes of HDPE and LDPE.

Further investigation into the misclassifications revealed that 6 of the 7 LDPE misclassifications came from one polymer, and 4 of the 5 HDPE misclassifications arose from a black colored HDPE. The singular PP misclassification was from a black PP. This finding demonstrates that classification *via* NIR still struggles with black colorants.^{16,23} However, it also offers

Table 4 Hyperparameters for the final LinearSVC models based on the averages of the Optuna nested-CV hyperparameters and those selected from the LOGO nested-CV process

Parameter name	Nested-CV value	LOGO value
<i>C</i>	57	110
<i>penalty</i>	"11"	"11"
<i>multi_class</i>	"ovr"	"ovr"
<i>class_weight</i>	Balanced	None
<i>max_iter</i>	500	10 000
<i>dual</i>	"Auto"	"Auto"
<i>tol</i>	"0.012"	0.015



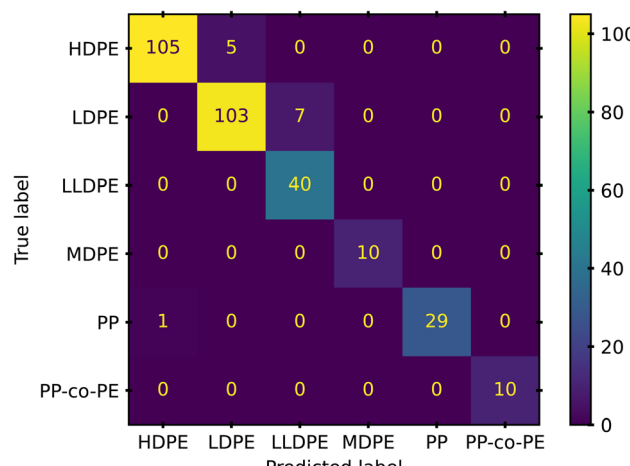


Fig. 7 A confusion matrix pairing true class and predicted class of the polymer samples. While HDPE and LDPE are the most consistently misclassified, they are also the largest contributions to our data set.

promise, as 16 of the 21 black samples were still properly classified. This indicates that there is potential for proper identification if there is enough data available to properly train models to recognize or ignore portions of the spectra that are altered by various additives. A larger study with more samples and a systematic representation of common additives may provide this level of refinement. The remaining 2 poor predictions arose from the recycled HDPE and LDPE samples. In both cases, the polymers could have degradation or contaminant artifacts from the recycling process. This seems especially likely for the LDPE that was consistently misclassified as LLDPE.

5 Conclusions

While more work must be done to build open and accessible databases to enable better sortation of polymeric waste, this work demonstrates the potential for a robust approach that can be applied easily by interested stakeholders. This work has thoroughly reviewed a wide variety of data preprocessing techniques to demonstrate that a simple RNV scattering correction and MinMaxScaler operation can successfully clean NIR spectra well enough to enable multiple machine learning algorithms to distinguish the highly similar PO classes with greater than 95% accuracy. This should enable more investigations, with more repeatable results, given that it eliminates overly complex or subjective corrections.

Additionally, this work has demonstrated that multiple classification algorithms can be tuned to enable rapid sortation of POs. This work chose LinearSVC as the preferred model due to its simplicity and high balanced accuracy scores. By using a LOGO CV method to tune the model, a more robust set of hyperparameters could be chosen to avoid both overfitting and enable generalizability. Our approach to refining the many variables in this study can also be used as a template for further research to limit the computational strain. This method enables a broad parameter search while avoiding wasted computational resources on unpromising parameter sets.

Example code and the data that were used to produce this work has been made public to enable further advances in the challenge of waste sortation.²⁶ We hope this approach to tuning classification models will be taken up by sortation equipment developers and applied by recyclers to improve the value and reuse of plastic waste recycling streams.

Data availability

The code and data for this manuscript can be found at <https://github.com/usnistgov/ECAPS> release 1.0.0. Additionally, the data used for this manuscript is being added to <https://data.nist.gov/> (DOI: <https://doi.org/10.18434/mds2-3022>) and should be release version 1.2.0 or 2.0.0.

Conflicts of interest

There are no conflicts to declare.

Acknowledgements

The authors thank the NIST Circular Economy program for financial support and Dr Kathryn Beers for helpful conversations. BPS thanks the NIST-NRC postdoctoral fellowship program and the NIST Information Technology Laboratory for support. The authors thank Dr Shailja Goyal and Rosine Yao for measurement data and kind assistance with characterization.

References

- 1 P. Liu, *et al.*, A comprehensive review on controlled synthesis of long-chain branched polyolefins: Part 1, single catalyst systems, *Macromol. React. Eng.*, 2016, **10**(3), 156–179, DOI: [10.1002/mren.201500053](https://doi.org/10.1002/mren.201500053).
- 2 G. Usanase, *et al.*, Determination of short chain branching in LLDPE by rheology, *Macromol. Chem. Phys.*, 2022, **223**(20), 2200150, DOI: [10.1002/macp.202200150](https://doi.org/10.1002/macp.202200150).
- 3 B. D. Vogt, K. K. Stokes and S. K. Kumar, Why is Recycling of Postconsumer Plastics so Challenging?, *ACS Appl. Polym. Mater.*, 2021, **3**(9), 4325–4346, DOI: [10.1021/acsapm.1c00648](https://doi.org/10.1021/acsapm.1c00648).
- 4 Wikipedia contributors, *Polyolefin*, <https://en.wikipedia.org/wiki/Polyolefin>, accessed: 24-09-2024.
- 5 P. Werner, 3 – Polyolefins, in *Applied Plastics Engineering Handbook*, ed. M. Kutz, William Andrew Publishing, Oxford, 2011, pp. 23–48, DOI: [10.1016/B978-1-4377-3514-7.10003-0](https://doi.org/10.1016/B978-1-4377-3514-7.10003-0), isbn: 9781437735147.
- 6 A. Van Belle, *et al.*, Microstructural Contributions of Different Polyolefins to the Deformation Mechanisms of Their Binary Blends, *Polymers*, 2020, **12**(5), 1171, DOI: [10.3390/polym12051171](https://doi.org/10.3390/polym12051171).
- 7 V. Busico and R. Cipullo, Microstructure of polypropylene, *Prog. Polym. Sci.*, 2001, **26**(3), 443–533, DOI: [10.1016/S0079-6700\(00\)00046-0](https://doi.org/10.1016/S0079-6700(00)00046-0).
- 8 B. P. Sutliff, *et al.*, Correlating near-infrared spectra to bulk properties in polyolefins, *Macromolecules*, 2024, **1520**–5835, DOI: [10.1021/acs.macromol.3c02290](https://doi.org/10.1021/acs.macromol.3c02290).

9 S. L. Aggarwal and O. J. Sweeting, Polyethylene: Preparation, Structure, And Properties, *Chem. Rev.*, 1957, **57**(4), 665–742, DOI: [10.1021/cr50016a004](https://doi.org/10.1021/cr50016a004).

10 D. W. Sauter, M. Taoufik and C. Boisson, Polyolefins, a Success Story, *Polymers*, 2017, **9**(6), 185, DOI: [10.3390/polym9060185](https://doi.org/10.3390/polym9060185).

11 D. B. Malpass and E. Band, *Introduction to Industrial Polypropylene: Properties, Catalysts Processes*, John Wiley & Sons, 2012. isbn: 9781118062760.

12 S. V. Orski, *et al.*, Design and Characterization of Model Linear Low-Density Polyethylenes (LLDPES) by Multidetector Size Exclusion Chromatography, *Macromolecules*, 2020, **53**(7), 2344–2353, DOI: [10.1021/acs.macromol.9b02623](https://doi.org/10.1021/acs.macromol.9b02623).

13 W. Wen-Jun, *et al.*, Triple-detector GPC characterization and processing behavior of long-chain-branched polyethylene prepared by solution polymerization with constrained geometry catalyst, *Polymer*, 2004, **45**(19), 6495–6505, DOI: [10.1016/j.polymer.2004.07.035](https://doi.org/10.1016/j.polymer.2004.07.035).

14 A. H. Westlie, *et al.*, Polyolefin Innovations toward Circularity and Sustainable Alternatives, *Macromol. Rapid Commun.*, 2022, **43**(24), e2200492, DOI: [10.1002/marc.202200492](https://doi.org/10.1002/marc.202200492).

15 S. Yin, *et al.*, Mechanical reprocessing of polyolefin waste: A review, *Polym. Eng. Sci.*, 2015, **55**(12), 2899–2909, DOI: [10.1002/pen.24182](https://doi.org/10.1002/pen.24182).

16 Z. O. G. Schyns and M. P. Shaver, Mechanical Recycling of Packaging Plastics: A Review, *Macromol. Rapid Commun.*, 2021, **42**(3), e2000415, DOI: [10.1002/marc.202000415](https://doi.org/10.1002/marc.202000415).

17 S. Serranti, A. Gargiulo and G. Bonifazi, Classification of polyolefins from building and construction waste using NIR hyperspectral imaging system, *Resour., Conserv. Recycl.*, 2012, **61**, 52–58, DOI: [10.1016/j.resconrec.2012.01.007](https://doi.org/10.1016/j.resconrec.2012.01.007).

18 S. Serranti, *et al.*, An innovative recycling process to obtain pure polyethylene and polypropylene from household waste, *Waste Manage.*, 2015, **35**, 12–20, DOI: [10.1016/j.wasman.2014.10.017](https://doi.org/10.1016/j.wasman.2014.10.017).

19 S. Serranti, *et al.*, “Characterization of microplastic litter from oceans by an innovative approach based on hyperspectral imaging”. en, *Waste Manage.*, 2018, **76**, 117–125, DOI: [10.1016/j.wasman.2018.03.003](https://doi.org/10.1016/j.wasman.2018.03.003).

20 C. Vidal and C. Pasquini, A comprehensive and fast microplastics identification based on near-infrared hyperspectral imaging (HSI-NIR) and chemometrics, *Environ. Pollut.*, 2021, **285**, 117251, DOI: [10.1016/j.envpol.2021.117251](https://doi.org/10.1016/j.envpol.2021.117251).

21 X. Yan, *et al.*, An ensemble machine learning method for microplastics identification with FTIR spectrum, *J. Environ. Chem. Eng.*, 2022, **10**(4), 108130, DOI: [10.1016/j.jece.2022.108130](https://doi.org/10.1016/j.jece.2022.108130).

22 H. Masoumi, S. M. Safavi and Z. Khani, Identification and classification of plastic resins using near infrared reflectance, *Int. J. Mech. Ind. Eng.*, 2012, **6**, 213–220.

23 M. Rani, *et al.*, Miniaturized Near-Infrared (MicroNIR) Spectrometer in Plastic Waste Sorting, *Materials*, 2019, **12**(17), 2740, DOI: [10.3390/ma12172740](https://doi.org/10.3390/ma12172740).

24 I. S. Helland, T. Næs and T. Isaksson, Related versions of the multiplicative scatter correction method for preprocessing spectroscopic data, *Chemom. Intell. Lab. Syst.*, 1995, **29**(2), 233–241, DOI: [10.1016/0169-7439\(95\)80098-T](https://doi.org/10.1016/0169-7439(95)80098-T).

25 Å. Rinnan, F. van den Berg and S. B. Engelsen, Review of the most common pre-processing techniques for near-infrared spectra, *TrAC, Trends Anal. Chem.*, 2009, **28**(10), 1201–1222, DOI: [10.1016/j.trac.2009.07.007](https://doi.org/10.1016/j.trac.2009.07.007).

26 B. P. Sutliff, S. Goyal, T. B. Martin, B. Tyler, P. A. Beauchage, D. J. Audus and S. V. Orski, *Correlating Near-Infrared Spectra to Bulk Properties in Polyolefins*, National Institute of Standards and Technology, 2023, DOI: [10.18434/mds2-3022](https://doi.org/10.18434/mds2-3022), accessed 2024-07-03.

27 Q. Guo, W. Wu and D. L. Massart, The robust normal variate transform for pattern recognition with near-infrared data, *Anal. Chim. Acta*, 1999, **382**(1), 87–103, DOI: [10.1016/S0003-2670\(98\)00737-5](https://doi.org/10.1016/S0003-2670(98)00737-5).

28 R. J. Barnes, M. S. Dhanoa and S. J. Lister, Standard normal variate transformation and DE-trending of near-infrared diffuse reflectance spectra, *Appl. Spectrosc.*, 1989, **43**(5), 772–777, DOI: [10.1366/0003702894202201](https://doi.org/10.1366/0003702894202201).

29 D. Iacobucci, *et al.*, Mean centering helps alleviate “micro” but not “macro” multicollinearity, *Behav. Res. Methods*, 2016, **48**(4), 1308–1317, DOI: [10.3758/s13428-015-0624-x](https://doi.org/10.3758/s13428-015-0624-x).

30 W. H. Press and S. A. Teukolsky, Savitzky-Golay Smoothing Filters, *Comput. Phys.*, 1990, **4**(6), 669–672, DOI: [10.1063/1.4822961](https://doi.org/10.1063/1.4822961).

31 A. Savitzky and M. J. E. Golay, Smoothing and differentiation of data by simplified least squares procedures, *Anal. Chem.*, 1964, **36**(8), 1627–1639.

32 F. Pedregosa, *et al.*, Scikit-learn: Machine Learning in Python, *J. Mach. Learn. Res.*, 2011, **12**, 2825–2830.

33 scikit-learn, <https://scikit-learn.org/stable/index.html>, accessed: 2023-10-27.

34 F. Corradini, *et al.*, Predicting soil microplastic concentration using vis-NIR spectroscopy, *Sci. Total Environ.*, 2019, **650**(Pt 1), 922–932, DOI: [10.1016/j.scitotenv.2018.09.101](https://doi.org/10.1016/j.scitotenv.2018.09.101).

35 E. R. Kai Neo, *et al.*, A review on chemometric techniques with infrared, Raman and laser-induced breakdown spectroscopy for sorting plastic waste in the recycling industry, *Resour., Conserv. Recycl.*, 2022, **180**, 106217, DOI: [10.1016/j.resconrec.2022.106217](https://doi.org/10.1016/j.resconrec.2022.106217).

36 L. McInnes, J. Healy and J. Melville, UMAP: Uniform Manifold Approximation and Projection for Dimension Reduction, *arXiv*, 2018, preprint, arXiv:1802.03426, DOI: [10.48550/arXiv.1802.03426](https://doi.org/10.48550/arXiv.1802.03426).

37 R. G. Brereton and G. R. Lloyd, Partial least squares discriminant analysis: taking the magic away, *J. Chemom.*, 2014, **28**(4), 213–225, DOI: [10.1002/cem.2609](https://doi.org/10.1002/cem.2609).

38 A. L. Pomerantsev and O. Y. Rodionova, Multiclass partial least squares discriminant analysis: Taking the right way—A critical tutorial, *J. Chemom.*, 2018, **32**(8), e3030, DOI: [10.1002/cem.3030](https://doi.org/10.1002/cem.3030).

39 L. C. Lee, C.-Y. Lioung and A. J. Abdul, Partial least squares-discriminant analysis (PLS-DA) for classification of high-dimensional (HD) data: a review of contemporary practice



strategies and knowledge gaps, *Analyst*, 2018, **143**(15), 3526–3539, DOI: [10.1039/c8an00599k](https://doi.org/10.1039/c8an00599k).

40 D. Ruiz-Perez, *et al.*, So you think you can PLS-DA?, *BMC Bioinf.*, 2020, **21**(Suppl 1), 2, DOI: [10.1186/s12859-019-3310-7](https://doi.org/10.1186/s12859-019-3310-7).

41 B. Ghojogh and M. Crowley, Linear and Quadratic Discriminant Analysis: Tutorial, *arXiv*, 2019, preprint, arXiv:1906.02590, DOI: [10.48550/arXiv.1906.02590](https://doi.org/10.48550/arXiv.1906.02590).

42 Y. Qin, A review of quadratic discriminant analysis for high-dimensional data, *Wiley Interdiscip. Rev. Comput. Stat.*, 2018, **10**(4), e1434, DOI: [10.1002/wics.1434](https://doi.org/10.1002/wics.1434).

43 L. Wang, *Support Vector Machines: Theory and Applications*, Springer Science & Business Media, 2005, isbn: 9783540243885.

44 V. Kecman, Support Vector Machines – An Introduction, in *Support Vector Machines: Theory and Applications. Studies in fuzziness and soft computing*, Springer Berlin Heidelberg, Berlin, Heidelberg, 2005, pp. 1–47, DOI: [10.1007/10984697_1](https://doi.org/10.1007/10984697_1).

45 A. Rácz, *et al.*, Is soft independent modeling of class analogies a reasonable choice for supervised pattern recognition?, *RSC Adv.*, 2017, **8**(1), 10–21, DOI: [10.1039/C7RA08901E](https://doi.org/10.1039/C7RA08901E).

46 O. Galtier, *et al.*, Comparison of PLS1-DA, PLS2-DA and SIMCA for classification by origin of crude petroleum oils by MIR and virgin olive oils by NIR for different spectral regions, *Vib. Spectrosc.*, 2011, **55**(1), 132–140, DOI: [10.1016/j.vibspec.2010.09.012](https://doi.org/10.1016/j.vibspec.2010.09.012).

47 S. Wold and M. Sjöström, SIMCA: A Method for Analyzing Chemical Data in Terms of Similarity and Analogy, in *Chemometrics: Theory and Application*, ACS Symposium Series, American Chemical Society, 1977, vol. 52, pp. 243–282, isbn: 9780841203792. doi: DOI: [10.1021/bk-1977-0052.ch012](https://doi.org/10.1021/bk-1977-0052.ch012).

48 A. Kelly and M. A. Johnson, Investigating the Statistical Assumptions of Naive Bayes Classifiers, in *2021 55th Annual Conference on Information Sciences and Systems (CISS)*, IEEE, 2021, pp. 1–6, DOI: [10.1109/CISS50987.2021.9400215](https://doi.org/10.1109/CISS50987.2021.9400215).

49 L. B. Almeida, Multilayer perceptrons, in *Handbook of Neural Computation*, CRC Press, 2020, pp. C1–C2.

50 A. J. Myles, *et al.*, An introduction to decision tree modeling, *J. Chemom.*, 2004, **18**(6), 275–285, DOI: [10.1002/cem.873](https://doi.org/10.1002/cem.873).

51 P. Virtanen, *et al.*, SciPy 1.0: Fundamental Algorithms for Scientific Computing in Python, *Nat. Methods*, 2020, **17**, 261–272, DOI: [10.1038/s41592-019-0686-2](https://doi.org/10.1038/s41592-019-0686-2).

52 C. Ramos-Carreño, *et al.*, scikit-fda: A Python Package for Functional Data Analysis, *arXiv*, 2022, preprint, arXiv:2211.02566, DOI: [10.48550/arXiv.2211.02566](https://doi.org/10.48550/arXiv.2211.02566).

53 Hawai'i Pacific University Center for Marine Debris Research, Polymers Kit 1.0, <https://www.hpu.edu/cnecs/cmdr/products-and-services.html>, accessed: 2023-5-30.

54 Any identification of software, equipment, instruments, companies, or materials in this work is done so for the express purposes of completeness and understanding. Such identification does not imply recommendation or endorsement by the National Institute of Standards and Technology, nor does it imply that the materials or equipment identified are necessarily the best available for the purpose.

55 Q. Duan and L. Jia, Classification of Common Household Plastic Wastes Combining Multiple Methods Based on Near-Infrared Spectroscopy, *ACS ES&T Eng.*, 2021, **1**(7), 1065–1073, DOI: [10.1021/acestengg.0c00183](https://doi.org/10.1021/acestengg.0c00183).

56 X. Yan, *et al.*, An ensemble machine learning method for microplastics identification with FTIR spectrums, 2023, <https://github.com/lyheiyu/An-ensemble-learning-for-microplastics-identification-with-FTIR/>.

57 M. Manjurul Ahsan, *et al.*, Effect of Data Scaling Methods on Machine Learning Algorithms and Model Performance, *Technologies*, 2021, **9**(3), 52, DOI: [10.3390/technologies9030052](https://doi.org/10.3390/technologies9030052).

58 S. Bates, T. Hastie and R. Tibshirani, Cross-validation: What does it estimate and how well does it do it?, *J. Am. Stat. Assoc.*, 2023, 1–12, DOI: [10.1080/01621459.2023.2197686](https://doi.org/10.1080/01621459.2023.2197686).

59 T. Akiba, *et al.*, Optuna: A Next-generation Hyperparameter Optimization Framework, in *Proceedings of the 25th ACM SIGKDD International Conference on Knowledge Discovery and Data Mining. KDD'19*, Anchorage, AK, USA, Association for Computing Machinery, 2019, pp. 2623–2631, DOI: [10.1145/3292500.3330701](https://doi.org/10.1145/3292500.3330701), isbn: 9781450362016.

60 Optuna Contributors, Efficient Optimization Algorithms – Optuna 3.6.1 documentation, accessed: 2024-4-3.

